

# Same-sign trilepton signal for stop quark in the presence of sneutrino dark matter

Dilip Kumar Ghosh\*

*Department of Theoretical Physics, Indian Association for the Cultivation of Science Jadavpur, Kolkata 700 032, India*

Katri Huitu<sup>†</sup> and Subhadeep Mondal<sup>‡</sup>

*Department of Physics, and Helsinki Institute of Physics,  
P. O. Box 64, FI-00014 University of Helsinki, Finland*

Manimala Mitra<sup>§</sup>

*Institute of Physics, Sachivalaya Marg, Bhubaneswar,  
Odisha 751005, India, Homi Bhabha National Institute,  
Training School Complex, Anushakti Nagar, Mumbai 400085, India*

We have explored a minimal supersymmetric standard model scenario extended by one pair of gauge singlets per generation. In the model light neutrino masses and their mixings are generated via inverse seesaw mechanism. In such a scenario, a right-handed sneutrino can be the lightest supersymmetric particle and a cold Dark Matter (DM) candidate. If Casas-Ibarra parametrisation is imposed on the Dirac neutrino Yukawa coupling matrix ( $Y_\nu$ ) to fit the neutrino oscillation data, the resulting  $Y_\nu$  is highly constrained from the lepton flavor violating (LFV) decay constraints. The smallness of  $Y_\nu$  requires the sneutrino DM to co-annihilate with other sparticle(s) in order to satisfy DM relic density constraint. We have studied sneutrino co-annihilation with wino and observed that this sneutrino-wino compressed parameter space gives rise to a novel same-sign trilepton signal for the stop quark, which is more effective than the conventional stop search channels in the present framework. We have shown that the choice of neutrino mass hierarchy strongly affects the signal event rate, making it easier to probe the scenario with inverted mass hierarchy.

arXiv:1807.07385v2 [hep-ph] 9 Apr 2019

---

\* tpdkg@iacs.res.in

† katri.huitu@helsinki.fi

‡ subhadeep.mondal@helsinki.fi

§ manimala@iopb.res.in

## I. INTRODUCTION

Existence of non-zero neutrino masses and mixings [1, 2] remain one of the unsolved puzzles and one of the strongest motivations for looking for physics beyond the Standard Model (BSM). Supersymmetry (SUSY) remains one of the frontrunners among various BSM candidates. However, the R-parity conserving minimal supersymmetric standard model (MSSM) is unable to address the neutrino mass problem. The easiest way to overcome this shortcoming is to incorporate a seesaw mechanism in the framework, where the light neutrinos gain non-zero masses through small mixing with additional gauge singlet fields. The canonical seesaw mechanism [3–7] introduces three generations of gauge singlet superfields to the MSSM particle contents. The light neutrino mass scale leads to very small Dirac neutrino Yukawa couplings ( $Y_\nu$ ) in the presence of TeV scale right-handed neutrinos. The smallness of  $Y_\nu$  makes it difficult to get any observable effect of the neutrino sector at the LHC. Lepton number and (or) lepton flavor violating (LFV) decays on the other hand, can constrain these parameters further with increasing sensitivities. A more phenomenologically interesting option is provided by the inverse seesaw mechanism [8–10] where the  $Y_\nu$  can in principle be as large as  $\mathcal{O}(0.1)$  owing to the presence of a small lepton number violating parameter in the theory. Such large Yukawa parameters and sub-TeV RH neutrino mass can be constrained from collider as well as low energy experiments [11–13].

Presence of a right-handed (RH) neutrino superfield in a SUSY theory provides us with an exciting possibility of obtaining a RH sneutrino as the lightest SUSY particle (LSP) which can also be a good cold Dark Matter (DM) candidate [14–25]. The left-handed sneutrino LSP option is strongly disfavored from DM direct detection constraint due to its gauge coupling with the  $Z$ -boson [26, 27]. A sub-TeV sneutrino LSP, in order to be considered as a DM candidate, therefore, has to be RH. This RH sneutrino arises from a singlet superfield and thus only couples to other particles via the Yukawa couplings. The DM experimental data can be another probe to test the neutrino sector parameters in models augmented with gauge singlet superfield. The only pair annihilation process of any significance involves Higgs bosons in the s-channel, and unless the sneutrino mass is close to the scalar resonance region, the annihilation is not enough to produce correct relic density [17–19]. Thus a sneutrino DM mass around  $\frac{m_h}{2}$ , where  $m_h$  indicates the 125 GeV Higgs boson mass, has been the favored region from the DM constraints. However, this region is now under severe scrutiny with the improvements in DM direct detection constraints.

In the absence of the Higgs resonance region, it is quite difficult to produce enough annihilation cross-section for the RH sneutrinos in such scenarios. This forces us to look at co-annihilation options. With proper co-annihilation, a sneutrino can be a viable DM candidate throughout the mass range [100 GeV - 1 TeV]. However, direct search constraints on the other sparticles indirectly put constraint on the sneutrino masses in such cases. Attractive options involve winos or higgsinos as next to lightest SUSY particle (NLSP) since they always present the possibility of co-annihilation with more than one particle simultaneously. Thus the DM constraints naturally leads to a compressed electroweak sector involving the LSP sneutrino and multiple neutralino-chargino states as the NLSP. As a result of this compression, the decay products of the NLSP neutralino-chargino are expected to be soft, resulting in weaker exclusion limits. This also means that such a scenario will be hard to detect from direct production of the NLSP pairs. One can, however, produce them in a cascade and look for a multilepton channel with small Standard Model (SM) background to distinguish the signal.

One such possibility can arise from stop quark production and its subsequent decay into the LSP sneutrino via the neutralino-charginos. The physics of stop quark is of utmost importance in the MSSM-like theories that require to add a substantial correction to the tree level Higgs boson mass in order to increase it up to 125 GeV. This correction appears mostly from stop quark loop making the stop masses and mixing parameters of interest in the search of SUSY at the LHC. The existing constraints on the stop quark masses can extend up to 1 TeV depending on its various decay modes [28–34]. At the same time this exclusion limit can be relaxed in presence of a compressed electroweak sector as we have here. It turns out that the existing search channels are not sensitive enough to probe stop masses effectively under such circumstances owing to the poor signal rates. Hence we have constructed a same-sign trilepton signal region, which is nearly background free and thus, despite of a poor event rate, can be used to probe TeV order stop masses at relatively low luminosity. We have also shown that the choice of normal hierarchy (NH) or inverted hierarchy (IH) in the light neutrino masses is reflected in the final event rate which draws a nice correlation between the neutrino and stop sector and also highlights a unique characteristic of such neutrino mass models.

The paper is organised as following. In section II, we briefly give an overview of the model and describe how neutrino oscillation data has been fit. In section III we discuss the phenomenological constraints on the model arising from LFV decays, DM and collider experiments. In section IV we discuss the canonical stop search strategies at the LHC and propose for the same a novel same-sign trilepton signal region, which is more suitable to probe the present scenario. Then we go on to define few benchmark points representative of the parameter space of our interest and perform a detailed collider analysis to present our results in the context of 13 TeV LHC. We have shown the exclusion limits on the stop mass derived from this study at moderate and high luminosities at the LHC in case of null result. In this context we have also presented the limits that can be expected at a high-energy (27 TeV) hadron machine. In

section V we summarise our results and conclude.

## II. MODEL

The supersymmetric inverse seesaw model (SISM) contains the SM gauge singlet superfields  $\hat{N}$  and  $\hat{S}$  with lepton numbers -1 and +1 respectively. The superpotential with these extra superfields is

$$W = W_{\text{MSSM}} + Y_\nu \hat{L} \cdot H_u \hat{N} + M \hat{N} \hat{S} + \mu_S \hat{S} \cdot \hat{S} \quad (2.1)$$

In the above we consider three generations of  $\hat{N}_i$  and  $\hat{S}_i$  ( $i=1,2,3$ ) and  $\mu_S$  violates lepton number by two units ( $\Delta L = 2$ ). The soft supersymmetry breaking Lagrangian for this model is

$$\mathcal{L}_{\text{soft}} = \mathcal{L}_{\text{MSSM}} - [m_N^2 \tilde{N} \tilde{N} + m_S^2 \tilde{S} \tilde{S}] - [A_\nu \tilde{L} H_u \tilde{N} + B_1 \tilde{N} \tilde{S} + B_2 \tilde{S} \tilde{S} + h.c.] \quad (2.2)$$

The  $9 \times 9$  neutrino mass matrix in the basis  $(\nu, N, S)$  has the following form,

$$\mathcal{M}_\nu = \begin{pmatrix} 0 & M_D & 0 \\ M_D^T & 0 & M \\ 0 & M^T & \mu_S \end{pmatrix} \quad (2.3)$$

where  $M_D$ ,  $M$  and  $\mu$  are  $3 \times 3$  matrix and  $M_D = Y_\nu v_u$ , where  $v_u$  is the vacuum expectation value (VEV) of  $H_u$ . For the parameter  $\|\mu_S\| \ll \|M\|$ , the light neutrino mass matrix becomes,

$$M_\nu \sim M_D M^{T-1} \mu_S M^{-1} M_D^T \quad (2.4)$$

The matrix  $\mu_S$  can be small<sup>1</sup> enough to explain the eV neutrino mass constraint. In passing we would like to add a few comments on the choice of our superpotential. Since we want the lightest right-handed sneutrino state to be a stable LSP and hence a DM candidate, we choose to work within R-parity conserving framework. This choice prevents us to write terms violating lepton number by odd unit(s), e.g.,  $\hat{N} \hat{N} \hat{N}$ ,  $\hat{N} \hat{N} \hat{S}$ ,  $\hat{S} \hat{S} \hat{S}$  and  $\hat{N} \hat{S} \hat{S}$ . We do not allow the scalar components of  $\hat{N}$  and  $\hat{S}$  to obtain VEVs for the same reason. However, one can in principle, allow additional  $\Delta L = 2$  terms, i.e., non-zero  $\hat{L} \hat{S}$  and  $\hat{N} \hat{N}$  terms in the superpotential. However, the presence of the  $\hat{N} \hat{N}$  term does not affect the inverse seesaw structure at tree-level as the rank of  $\mathcal{M}_\nu$  remains same. On the other hand, the  $\hat{L} \hat{S}$  term will modify eq. 2.4 unless the coupling  $Y_S$  in  $Y_S \hat{L} \cdot \hat{H}_u \hat{S}$  is very small,  $Y_S \lesssim 10^{-12}$ . One can impose additional symmetry [36, 37] in the superpotential to forbid such terms. We have chosen to work within a minimal set up [38–41] that can address the neutrino oscillation data via inverse seesaw mechanism.

The light neutrino mass matrix is diagonalized by the PMNS mixing matrix  $U_\nu$  as follows.

$$U_\nu^T M_\nu U_\nu^* = M_\nu^d \quad (2.5)$$

We consider the matrices  $M$  and  $\mu_S$  to be diagonal. One can follow the Casas-Ibarra parametrization [42] to construct the matrix  $R$

$$R = M_\nu^{d-1/2} U_\nu^T M_D M^{T-1} \mu_S^{1/2}, \quad (2.6)$$

where  $R$  is a complex orthogonal matrix with  $RR^T = I$ . Throughout the paper, we consider the best fit values of the oscillation parameters [2]. The Dirac mass matrix  $M_D$  can be fixed in terms of the light neutrino masses, PMNS mixing matrix and  $R$  as

$$M_D = U_\nu^* \sqrt{M_\nu^d} R \mu_S^{-1/2} M \quad (2.7)$$

In our subsequent discussion, we consider the simplest scenario with  $R = \mathbb{I}$ . The heavy neutrino masses are proportional to  $M \pm \mu_S$ . After diagonalization, this gives rise to the quasi-degenerate sterile neutrino states with mass splitting  $\delta M \sim \mu_S$ .

Below, we discuss a number of experimental constraints arising from the lepton flavor violating searches, dark matter searches and collider constraints.

<sup>1</sup> Note that,  $\mu_S$  breaks lepton number by two units. Hence in the limit  $\mu_S \rightarrow 0$ , the symmetry of the theory enhances. From the naturalness argument,  $\mu_S$  is preferred to be small. Moreover, a small  $\mu_S$  is absolutely essential to incorporate inverse seesaw mechanism. Moreover, a large  $\mu_S$  will cause the  $\Delta L = 2$  processes like neutrinoless double beta decay rate to increase rapidly [35].

### III. EXPERIMENTAL CONSTRAINTS

In this section, we discuss different experimental constraints on the heavy neutrino and sneutrino parameters in addition to the neutrino oscillation data. The heavy neutrinos in the inverse seesaw can give large contribution in the loop mediated LFV process  $\ell_i \rightarrow \ell_j \gamma$ ,  $\ell_i \rightarrow \ell_j \ell_j \ell_j$  and  $\ell_i \rightarrow \ell_j$  conversion in nuclei [38–41, 43, 44]. Additionally, for much lower masses upto few GeV, the sterile neutrinos can further be constrained from different LFV meson decays  $M \rightarrow M' \ell_i \ell_j$ , fixed target experiments, the peak searches in  $\pi \rightarrow e \nu$  and  $K \rightarrow e \nu$ , as well as  $\beta$  decay [45]. Active-sterile neutrino mixing upto  $\theta^2 \sim 10^{-11}$  can be probed in future FCC-ee [46] and SHiP [47], relevant for few GeV mass range of the RH neutrino. SISM is augmented with small lepton number violation owing to the smallness of  $\mu_S$ . Therefore, the LNV processes, such as  $0\nu 2\beta$ , LNV meson decays  $K \rightarrow \pi l^\pm l^\pm$  will be suppressed in this model. We consider the heavy neutrinos in the [100 GeV - 1 TeV] range that can be most optimally tested through the flavor violation and collider searches. In the SISM,  $\ell_i \rightarrow \ell_j \gamma$  and  $\ell_i \rightarrow \ell_j$  conversion in nuclei are further enhanced due to sneutrino-chargino and slepton-neutralino mediated loop contributions. We furthermore assume that the sneutrino is the LSP and obtain the constraints from the dark matter relic density.

#### LFV Constraints

As an artefact of fitting the neutrino oscillation data as described in the previous section, the resulting Dirac neutrino mass matrix,  $M_D$ , becomes off-diagonal which can potentially enhance LFV decays like  $\ell_i \rightarrow \ell_j \gamma$ . We keep the Yukawa matrix for the charged lepton diagonal. As a result, the LFV decays are generated at one loop through contributions from lepton-neutrino-W boson, lepton-slepton-neutralino and lepton-sneutrino-chargino loops. Both these non-supersymmetric and supersymmetric loop contributions have been studied in detail [38, 41, 48]. Depending on the choices of the neutrino sector parameters, namely,  $M_D$ ,  $M$ ,  $\mu_S$  and the chargino and sneutrino masses, these LFV decay rates can be significant. The experimental limits on such LFV decay branching ratios [49–55] thus can restrict the model parameter space effectively. The existing constraints are more stringent for LFV decays of muons than of taus owing to better detection efficiency of the former. Hence stringent restrictions on the  $Y_\nu$  parameters are to be expected when inverted hierarchy among the light neutrino masses are considered owing to the resultant large  $Y_\nu$  corresponding to the first generation. In order to study the impact of these constraints on the LSP mass and its couplings, we have performed a scan where  $M$  has been varied within the range [100 GeV - 1 TeV]. Wino mass parameter  $M_2$  has been adjusted in such a way that  $m_{\tilde{\nu}_{1,2}} < m_{\tilde{\chi}_1^\pm} \leq m_{\tilde{\nu}_{1,2}} + 50$  GeV to facilitate co-annihilation with the LSP, which has been discussed in the subsequent subsection. The value of  $\tan\beta$  has been kept fixed at 10 and different  $\mu_S$  values ( $10^{-8}$ ,  $10^{-7}$  and  $10^{-6}$  GeV) have been chosen with  $Y_\nu$  fitted according to Eq. 2.7. The computation of particle masses, mixing and their decay have been performed using SPheno<sup>2</sup> [56–58] after model implementation using SARAH [59–63]. For the LFV decay branching ratio calculations we have used the results from ref. [41] which include both the SUSY and non-SUSY contributions.

Fig. 1 shows the variation of the relevant LFV decay branching ratios as a function of the LSP mass  $m_{\tilde{\nu}_{1,2}}$ <sup>3</sup>. The different colored lines correspond to different choices of  $\mu_S$  while the black solid and dotted lines represent the present and future experimental sensitivities for the respective LFV processes. As expected, the constraints are most severe for the IH case in the  $\mu \rightarrow e \gamma$  and  $\mu N \rightarrow e N^*$  modes. In particular, for IH in the light neutrino masses, the LNV parameter  $\mu_S < 10^{-6}$  GeV is excluded throughout the entire LSP mass region upto  $\tilde{m}_\nu = 1000$  GeV. The restriction is relatively much weaker from LFV  $\tau$  decays,  $\tau \rightarrow e \gamma$ ,  $\tau \rightarrow \mu \gamma$  and  $\tau \rightarrow \mu \mu \mu$ . The experimental limits on these decay modes are yet to improve significantly to probe the parameter space in consideration. As expected, for the  $\tau$  LFV decays, NH mass hierarchy predicts a larger branching ratio than the IH mass hierarchy because of the largeness in third generation Yukawa couplings. This is easily testable in the next generation experiments. With the recent results of the neutrino oscillation experiment *Nova* disfavoring IH in neutrino sector [64, 65], the predictions for NH are even more significant. For  $\tau \rightarrow e \gamma$  the predicted branching ratio is smaller by more than  $\mathcal{O}(10^4)$  than  $\tau \rightarrow \mu \gamma$ . In this case, both the lines corresponding to NH and IH merge to result in one unique line for each  $\mu_S$  values<sup>4</sup>. The restriction from  $\tau \rightarrow e e e$  is the weakest, and hence we do not explicitly show that. As the future sensitivities show,  $\mu N \rightarrow e N^*$  conversion process is most likely to probe this parameter space entirely.

Apart from the neutrino sector parameters, the masses of the neutralino and charginos can also be constrained from these LFV decay computations. In order to get Fig. 1, we have only kept the wino mass close to the LSP as mentioned above. All other neutralino-chargino masses are kept above 2.0 TeV. Since the wino pair lie close to the LSP mass,

<sup>2</sup> All the masses are calculated with corrections upto one loop, apart from the Higgs mass which is computed upto two loop level.

<sup>3</sup> Heavy neutrino masses are same as the sneutrino masses since they are both driven by the same parameter  $M$ .

<sup>4</sup> In the distributions of  $BR(\tau \rightarrow \mu \gamma)$  and  $BR(\tau \rightarrow \mu \mu \mu)$ , the IH lines corresponding to the smaller  $\mu_S$  overlaps with the NH line corresponding to the subsequent  $\mu_S$ . The small numerical difference between the lines is indistinguishable in the logarithmic scales of the figures.

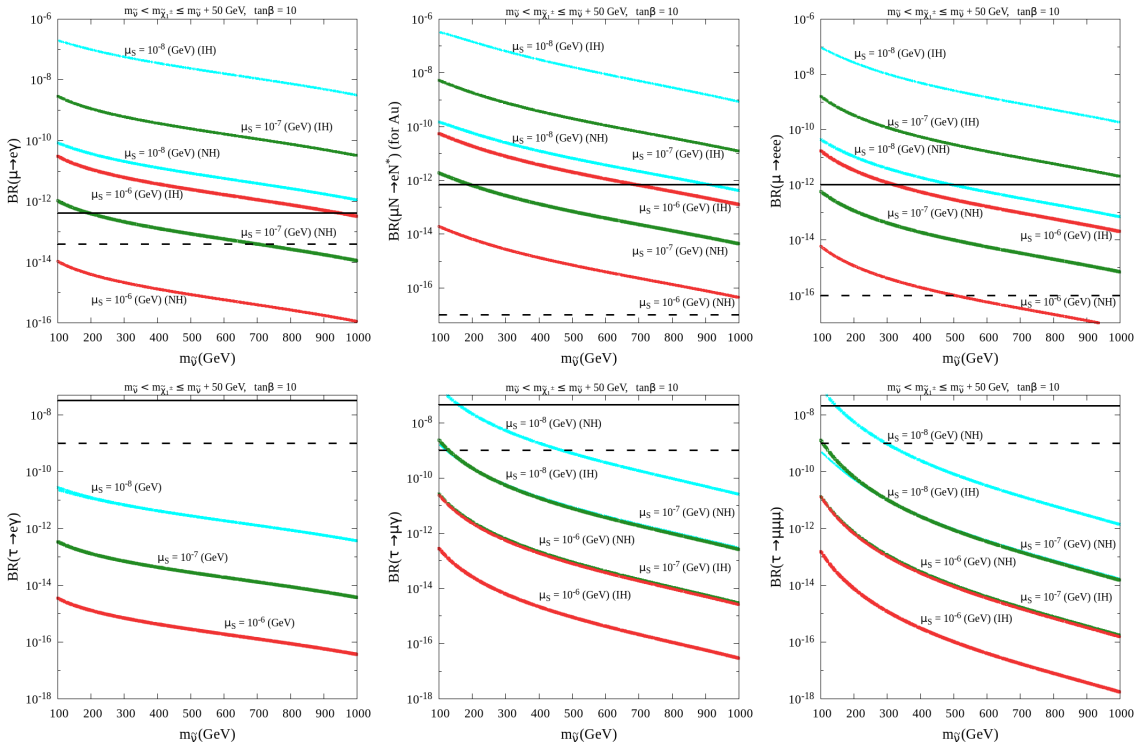


FIG. 1. Top panel: the predicted branching ratio of  $\mu \rightarrow e\gamma$ ,  $\mu - e$  conversion in nuclei and  $\mu \rightarrow eee$  vs the sneutrino mass. Lower panel: the branching ratio for  $\tau \rightarrow e\gamma$ ,  $\tau \rightarrow \mu\gamma$  and  $\tau \rightarrow \mu\mu\mu$ . The horizontal solid black line corresponds to the present experimental bounds on  $\text{BR}(\mu \rightarrow e\gamma) \leq 4.2 \times 10^{-13}$ ,  $\text{BR}(\mu N \rightarrow e N^*) \leq 10^{-12}$ ,  $\text{BR}(\mu \rightarrow eee) \leq 10^{-12}$ ,  $\text{BR}(\tau \rightarrow e\gamma) \leq 3.3 \times 10^{-8}$ ,  $\text{BR}(\tau \rightarrow \mu\gamma) \leq 4.4 \times 10^{-8}$  and  $\text{BR}(\tau \rightarrow \mu\mu\mu) \leq 2.1 \times 10^{-8}$  [49–55]. The corresponding future sensitivities are shown by the horizontal dotted black lines [49–55].

some of the parameter region with light enough sneutrino mass can be ruled out from the LHC data. However, LFV constraints on these masses depend on the choice of  $\mu_S$ . As shown in Fig. 1, large  $\mu_S$  results in weaker LFV constraint. We checked that for  $\mu_S \sim 10^{-5}$  GeV, even for more constraining inverted hierarchy scenario, sneutrino and chargino masses close to 200 GeV are still allowed from the LFV decays. However, that parameter space will be ruled out from LHC direct search constraints on the gaugino masses. Note that, LFV decay rates are not significant enough to constrain SUSY particle masses above 100 GeV for  $\mu_S \gtrsim 10^{-6}$  GeV if the light neutrino masses are aligned in normal hierarchy.

### Dark Matter Constraints

In the SISM, a light RH sneutrino cold DM candidate can be ideally fit in the Higgs resonance region [17–19], i.e.,  $m_{\tilde{\nu}_{1,2}}$  requires to lie in the vicinity of  $m_h/2$ , where  $m_h$  is the SM-like Higgs mass in order to ensure enough annihilation to satisfy the relic density constraint [66]. The RH sneutrino states are required to have sufficiently small mixing with the LH sneutrino states in order to avoid the direct detection cross-section ( $\sigma_{SI}$ ) constraints. However, the most recent constraint on  $\sigma_{SI}$  imposed by DM experiments like XENON1T and PANDA [67–69] have already excluded this parameter space. On the other hand, imposing the LFV constraints on the LSP mass and couplings renders the  $Y_\nu$  parameters sufficiently small so that the resulting  $\sigma_{SI}$  in the sub-TeV  $\tilde{\nu}_{1,2}$  mass region lies orders of magnitude below the present experimental sensitivity [67–69]. However, such small  $Y_\nu$  implies that even the Higgs resonance region can not provide sufficient annihilation for the RH-sneutrino LSP to satisfy the relic density constraint. As a consequence, one has to look for co-annihilation of  $\tilde{\nu}_{1,2}$  with other sparticles. Here we have studied the sneutrino co-annihilation with wino-like chargino and neutralino. The right-handed LSP sneutrino can not interact directly with the wino components of the chargino-neutralino pair and can only do so through their higgsino component. However, we have studied the case where the NLSP chargino-neutralino pair are almost purely wino-like. Under this circumstance, the resultant relic density is entirely due to the co-annihilation of the chargino-neutralino pair. The contribution of sneutrino annihilation to the relic density is negligibly small [70]. Hence, the LSP can be purely right-handed,

that results in elusively small direct detection cross-section. We have use MicrOmegas [71] for the calculation of relic density and direct detection cross-section.

It is worth mentioning that a higgsino NLSP can also be a good choice. Due to the presence of three nearly degenerate neutralino-chargino states that can co-annihilate with the sneutrino, a higgsino NLSP scenario is also capable of producing the correct relic density with appropriate choice of the higgsino parameters. A bino LSP scenario, on the other hand, fail to meet the relic density criteria due to lack of sufficient co-annihilation channels.

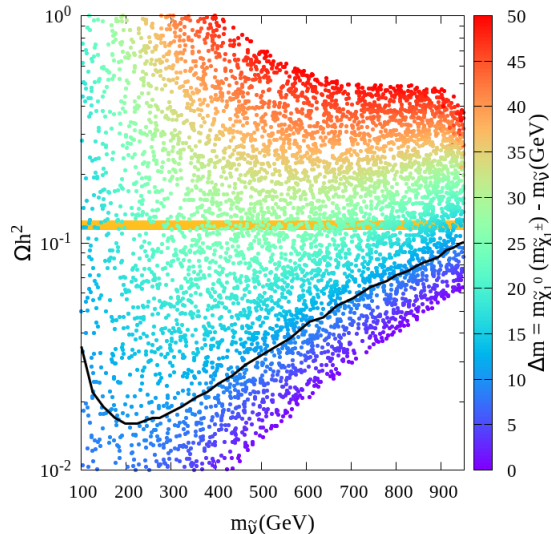


FIG. 2. The variation of the relic density is shown as a function of the LSP sneutrino mass. The color coding represents the LSP-NLSP mass gap,  $\Delta m$ . The horizontal band represents  $2\sigma$  allowed range of relic density,  $\Omega h^2 = 0.119 \pm 0.0027$  [66]. The black contour represents  $\Delta m \sim 10$  GeV.

Fig. 2 shows the relic density ( $\Omega h^2$ ) distribution as a function of DM mass,  $m_{\tilde{\nu}_{1,2}}$  after taking into account neutrino mass and LFV constraints.  $\tan\beta$  is kept fixed at a moderate value,  $10^5$  and the  $Y_\nu$  matrix is derived at each point according to Eq. 2.7. The NH or IH choices do not have significant impact on the distribution. However, we keep  $\mu_S = 10^{-5}$  GeV in order to be safe from the LFV constraints. The parameter  $M$  has been varied in the range [100 - 1000] GeV as before and to ensure co-annihilation the LSP-NLSP mass difference ( $\Delta m = m_{\tilde{\chi}_1^0} - m_{\tilde{\nu}_{1,2}}$ ) have been kept within 50 GeV by adjusting the wino mass parameter,  $M_2$ . The  $\Delta m$  variation is color coded according to the gradient bar on the right. The horizontal golden shaded region indicates the  $2\sigma$  allowed range of relic density,  $\Omega h^2 = 0.119 \pm 0.0027$  [66]. As evident from the figure,  $15 < \Delta m < 30$  GeV is favored from  $\Omega h^2$  consideration. Therefore, one can derive stringent constraint on the NLSP masses subjected to the sneutrino DM mass from relic density requirement. The black contour in Fig. 2 shows the boundary below which  $\Delta m < 10$  GeV. With such small  $\Delta m$ , the decay products of the NLSP will practically be undetectable. However, in this work, we are only concerned with the points lying over the relic density allowed band. Given the allowed  $\Delta m$  corresponding to these points, the resulting NLSP decay products will be soft but detectable with varied efficiency <sup>6</sup>.

### Collider Constraints

Since the sneutrino DM requires co-annihilation with a wino in the present scenario, the existing limits on the mass of wino-like chargino and neutralino can further constrain the DM allowed parameter region indirectly. The most stringent constraints from LHC on the wino mass is derived from trilepton and(or) dilepton final states resulting from  $\tilde{\chi}_2^0 \tilde{\chi}_1^\pm$  and  $\tilde{\chi}_1^\pm \tilde{\chi}_1^\mp$  production channels, respectively, with the assumption that  $\tilde{\chi}_2^0$  and  $\tilde{\chi}_1^\pm$  are wino-like and mass degenerate while the  $\tilde{\chi}_1^0$  is the LSP and is bino-like [72–78]. However, in our scenario the wino-bino mass hierarchy is reversed and sneutrino being the LSP, the final decay products are kinematically quite different. The co-annihilation requirement puts the wino  $\tilde{\chi}_1^0 \tilde{\chi}_1^\pm$  pair close to the  $\tilde{\nu}_{1,2}$  mass and as a result, the leptons arising from the  $\tilde{\chi}_1^\pm$  decay

<sup>5</sup> Choice of  $\tan\beta$  does not impact the sneutrino mass range or the LSP-NLSP mass gap required to produce correct relic density.

<sup>6</sup> In our collider analysis, in order to attain maximal cut efficiency, we have considered  $\Delta m \sim 25$  GeV.

are quite soft.  $\tilde{\chi}_1^0$  on the other hand, decays completely invisibly. Besides, the  $\tilde{\chi}_2^0\tilde{\chi}_1^\pm$  production cross-section is much smaller here compared to that used by the experimental analyses because of the sizable mass gap between the two states.  $\tilde{\chi}_1^\pm\tilde{\chi}_1^0$  production cross-section is expected to be larger, but the mono-lepton signal has a huge background contribution arising from single  $W$  production channel at the LHC. Thus the neutralino-chargino production channels result in much weaker limits on the relevant sparticle masses. Existing constraints from  $\tilde{\chi}_1^\pm\tilde{\chi}_1^\mp$  production can also restrict the SISM scenario. However, the resultant dilepton signal region requires relatively large lepton  $p_T$  cuts that reduces the signal event rate drastically in our case. One can revisit the dilepton analyses of ATLAS and CMS in this regard with softer  $p_T$  cuts on the leptons. Nevertheless, one has to use a large stransverse mass ( $M_{T2}$ ) cut in order to get rid of the background arising from  $W$  boson pair production. This cut discards most of the signal events from chargino pair production here because of the small chargino-sneutrino mass gap. Moreover, the absence of large transverse missing energy makes this channel less sensitive at the LHC. The existing exclusion limits are clearly not sensitive when LSP-NLSP mass gap is  $\sim 20 - 30$  GeV even with small  $M_{T2}$  cuts [72]. All these factors combine to make the existing limits on the gaugino masses much more relaxed in our case and allow us to choose sufficiently light sneutrino DM masses. We have ensured that the existing constraints on the gaugino masses are properly taken into account by testing our parameter space against the LHC results via CheckMATE [79, 80].

#### IV. COLLIDER PHENOMENOLOGY

Our discussion of the SISM scenario and the impact of the neutrino oscillation, LFV and DM experimental constraints point towards a naturally compressed spectrum consisting of the LSP sneutrino and the NLSP wino-like neutralino-chargino pair. As discussed in the previous section, the canonical search strategy for the gauginos at the LHC may not be sensitive enough to probe this scenario or distinguish the signal from that expected from a MSSM compressed spectra. We observe that a clean and distinguishable signal region for our scenario can be obtained via secondary production of the gauginos from a stop cascade. Note that, although the choices of wino masses in this framework are subjected to the choice of the LSP mass, the bino-like neutralino ( $\tilde{\chi}_2^0$ ) and the colored sparticle masses lie anywhere as long as they are not excluded by the LHC data.

The stop quark search at the LHC [29–34] mostly concentrates on the two stop decay modes  $\tilde{t} \rightarrow t\tilde{\chi}_1^0$  and  $\tilde{t} \rightarrow \tilde{\chi}_1^\pm b$ , where  $\tilde{\chi}_1^0$  and  $\tilde{\chi}_1^\pm$  are bino and wino-like, respectively. The various signal regions include 0, 1 or 2 lepton final states associated with  $b$ -jets and missing transverse energy ( $\cancel{E}_T$ ). The most stringent constraint on the stop masses in the MSSM framework is derived assuming either  $\tilde{t} \rightarrow t\tilde{\chi}_1^0$ ,  $\tilde{t} \rightarrow b\tilde{\chi}_1^\pm$  ( $\tilde{\chi}_1^\pm \rightarrow W\tilde{\chi}_1^0$ ) or  $\tilde{t} \rightarrow bf\tilde{\chi}_1^0$ , where  $f$  refers to the fermions. The existing bound on the stop masses can extend upto 1 TeV for a massless LSP [32, 33]. Although similar final states can be obtained in our scenario, these conventional decay branching ratios can be quite small and at the same time, the leptons originating from the NLSP decay  $\tilde{\chi}_1^\pm \rightarrow \ell\tilde{\nu}_{1,2}$  are expected to be soft and consequently result in worse cut efficiency. Thus the conventional search strategies for the lighter stop may not be applicable to probe this scenario.

A very clean and unique final state can result from right-handed stop pair production and subsequent decay of a stop into a bino-like  $\tilde{\chi}_2^0$  along with a top quark, while  $\tilde{\chi}_2^0$  further decays to the wino-like chargino  $\tilde{\chi}_1^\pm$  and a  $W$ -boson. The  $\tilde{\chi}_1^\pm$  finally decays to a charged lepton and LSP sneutrino. Owing to the Majorana nature of the  $\tilde{\chi}_2^0$ , this cascade can result at LHC in a same-sign tri-lepton signal, which is almost background free. The full-decay chain that we consider here is, therefore, as follows:

$$pp \rightarrow \tilde{t}_1\tilde{t}_1^* \rightarrow t\tilde{\chi}_2^0\bar{t}\tilde{\chi}_2^0 \rightarrow bW^+\bar{b}W^-\tilde{\chi}_1^\pm\tilde{\chi}_1^\pm W^\mp W^\mp; \quad \tilde{\chi}_1^\pm \rightarrow \ell^\pm\tilde{\nu}_{1,2}$$

Final state consists of  $b\bar{b} + n - \text{jets} + \ell^\pm\ell^\pm\ell^\pm + \cancel{E}_T$  ( $\ell \equiv e, \mu$ ), where two of the same-sign leptons originate from the two charginos while the third originates from one of the  $W$ -bosons arising from top quark decays. Note that, a similar hierarchy in the stop and gaugino masses can be obtained in the MSSM as well with wino-like LSP. However, in that case, in order to result in a same-sign trilepton final state, three of the same-sign  $W$ -bosons in the cascade would have to decay leptonically. The final event rate is, therefore, expected to be less [28] due to the small  $W$  leptonic decay branching ratio. However, in our present scenario, the NLSP  $\tilde{\chi}_1^\pm$  can only decay leptonically ( $e, \mu$  or  $\tau$ ) into the sneutrino and only one of the  $W$ s in the cascade is required to do the same. Hence the event rate is expected to be much larger. On the other hand, the LSP-NLSP compressed region ( $\Delta m \simeq 25 - 30$  GeV) results in softer leptons, which affects the cut efficiency and dents the event rate somewhat, but the same-sign trilepton being a clean channel, proves to be much more effective in probing the SISM parameter space than the conventional signal regions.

### A. Sample benchmark points

In Table I below, we have presented the relevant parameters, masses, branching ratios and different experimental constraints corresponding to two sample benchmark points assuming NH and IH in each cases.

Parameters, masses & Branching Ratios	BP1			BP2		
	Normal	Inverted		Normal	Inverted	
$M_1$ (GeV)	530.0	530.0		740.0	740.0	
$M_2$ (GeV)	401.1	401.1		595.8	595.8	
$M_{\tilde{t}_L}^2$ (GeV <sup>2</sup> )	$6.0 \times 10^6$	$6.0 \times 10^6$		$6.0 \times 10^6$	$6.0 \times 10^6$	
$M_{\tilde{t}_R}^2$ (GeV <sup>2</sup> )	$5.5 \times 10^5$	$5.5 \times 10^5$		$8.0 \times 10^5$	$8.0 \times 10^5$	
$\mu$ (GeV)	1500.0	1500.0		1500.0	1500.0	
$A_t$ (GeV)	-2200.0	-2200.0		-2200.0	-2200.0	
$\tan\beta$ (GeV)	10.0	10.0		10.0	10.0	
$M^{11}$ (GeV)	400.0	400.0		600.0	600.0	
$\mu_S^{ii}$ (GeV)	$10^{-5}$	$10^{-5}$		$10^{-5}$	$10^{-5}$	
$Y_\nu (\times 10^2)$	$\begin{pmatrix} 0.019 & -0.264 & 0.362 \\ 0.013 & 0.303 & -0.805 \\ 0.003 & 0.358 & 0.949 \end{pmatrix}$	$\begin{pmatrix} 0.425 & -0.636 & 0.016 \\ 0.281 & 0.730 & -0.036 \\ 0.076 & 0.862 & 0.042 \end{pmatrix}$		$\begin{pmatrix} 0.029 & -0.264 & 0.362 \\ 0.019 & 0.303 & -0.805 \\ 0.005 & 0.357 & 0.949 \end{pmatrix}$	$\begin{pmatrix} 0.637 & -0.636 & 0.016 \\ 0.421 & 0.730 & -0.036 \\ 0.114 & 0.862 & 0.042 \end{pmatrix}$	
$m_{\tilde{t}_1}$ (GeV)	860.1	860.1		994.8	994.8	
$m_{\tilde{\chi}_1^\pm}$ (GeV)	426.7	426.7		627.3	627.3	
$m_{\tilde{\chi}_2^0}$ (GeV)	530.9	530.9		741.6	741.6	
$m_{\tilde{\chi}_1^0}$ (GeV)	426.5	426.5		627.1	627.1	
$m_{\tilde{\nu}_{1,2}}$ (GeV)	400.0	400.0		600.0	600.0	
$m_N$ (GeV)	400.0	400.0		600.0	600.0	
$\text{BR}(\tilde{t}_1 \rightarrow \tilde{\chi}_2^0 t)$	0.89	0.89		0.84	0.84	
$\text{BR}(\tilde{t}_1 \rightarrow \tilde{\chi}_1^0 t)$	0.03	0.03		0.05	0.05	
$\text{BR}(\tilde{t}_1 \rightarrow \tilde{\chi}_1^\pm b)$	0.08	0.08		0.11	0.11	
$\text{BR}(\tilde{\chi}_2^0 \rightarrow \tilde{\chi}_1^\pm W^\mp)$	0.99	0.99		0.99	0.99	
$\text{BR}(\tilde{\chi}_2^\pm \rightarrow \tilde{\nu}_{1,2} e)$	-	0.31		-	0.50	
$\text{BR}(\tilde{\chi}_1^\pm \rightarrow \tilde{\nu}_{1,2} \mu)$	0.35	0.69		0.35	0.50	
$\text{BR}(\tilde{\chi}_1^\pm \rightarrow \tilde{\nu}_{1,2} \tau)$	0.65	-		0.65	-	
$\text{BR}(\mu \rightarrow e\gamma)$	$4.5 \times 10^{-18}$	$1.3 \times 10^{-14}$		$1.4 \times 10^{-18}$	$4.0 \times 10^{-15}$	
$\text{BR}(\mu N \rightarrow eN)$ (Au)	$5.1 \times 10^{-18}$	$1.5 \times 10^{-14}$		$1.1 \times 10^{-18}$	$3.3 \times 10^{-15}$	
$\text{BR}(\tau \rightarrow e\gamma)$	$1.5 \times 10^{-18}$	$1.5 \times 10^{-18}$		$4.6 \times 10^{-19}$	$4.5 \times 10^{-19}$	
$\text{BR}(\tau \rightarrow \mu\gamma)$	$2.9 \times 10^{-16}$	$3.4 \times 10^{-18}$		$3.9 \times 10^{-17}$	$4.5 \times 10^{-19}$	
$\Omega h^2$ (GeV)	0.120	0.120		0.120	0.120	
$\sigma_{SI}$ (pb)	$8.8 \times 10^{-18}$	$8.8 \times 10^{-18}$		$2.0 \times 10^{-19}$	$2.0 \times 10^{-19}$	
$pp \rightarrow \tilde{t}_1 \tilde{t}_1$ (fb)	17.55	17.55		6.38	6.38	

TABLE I. Relevant parameters, masses and branching ratios along with relic density, direct detection cross-section and stop pair production cross-section at 13 TeV LHC corresponding to the two benchmark points for both NH and IH of light neutrino masses.  $\mu_S^{ii}$  represents the three diagonal entries of the matrix  $\mu_S$  and  $M^{11}$  represents the first generation diagonal entry in the matrix  $M$ . The other two diagonal entries  $M^{22}$  and  $M^{33}$  are kept fixed at 1000 GeV.

For our choice of the sneutrino mass and lepton number violating parameter  $\mu_S$ , the LFV branching ratios are well within the present experimental limits, and the IH case of BP1 is the one closest to be probed by  $\text{BR}(\mu \rightarrow e\gamma)$  in near future. The DM direct detection cross-sections are also rendered quite small. The choice of NH or IH is highlighted in the resulting  $Y_\nu$  matrix. The larger third generation  $Y_\nu$  results in larger decay BR of the  $\tilde{\chi}_1^\pm$  into  $\tau\tilde{\nu}_{1,2}$  in the NH case. On the other hand, in the IH case, larger first generation  $Y_\nu$  leads to a larger  $\text{BR}(\tilde{\chi}_1^\pm \rightarrow e\tilde{\nu}_{1,2})$ . Naturally, one would expect larger leptonic event rates in the IH cases compared to the NH ones when the lighter chargino appears in the cascade. The  $\tilde{t}_1$ , being mostly right-handed, decays dominantly into a top quark and the bino-like  $\tilde{\chi}_2^0$ . In the absence of the  $\tilde{\chi}_1^0 h$  mode,  $\tilde{\chi}_2^0$  decays entirely into  $\tilde{\chi}_1^\pm W^\mp$ . The mass difference between  $\tilde{\chi}_2^0$  and  $\tilde{\chi}_1^0$  is chosen to ensure this so that the largest possible signal rate can be estimated.

Note that, the key difference in between **BP1** and **BP2** lies in the choices of the lighter stop and the LSP sneutrino mass. The relevant branching ratios of the  $\tilde{\chi}_2^0$  and  $\tilde{t}_1$  are similar in both the benchmark points.  $\text{BR}(\tilde{\chi}_1^\pm \rightarrow \ell\tilde{\nu}_{1,2})$ , where  $\ell = e$  or  $\mu$ , slightly differ in the IH case due to the resultant  $Y_\nu$  matrix with comparatively bigger  $Y_\nu^{11}$  required to fit the neutrino oscillation data subjected to the choice of  $M^{11}$ .



## B. Analysis and future reach

We have simulated pair production of RH stop quarks and its subsequent decays as already discussed for the two above mentioned benchmark points. The events were generated at the parton level using MadGraph v2.5.5 [81, 82] and subsequently passed through Pythia8 [83] for decay, showering and hadronization. We have used nn23lo1 parton distribution function [84, 85]. Detector simulation was implemented via Delphes v3.4.1 [86–88]. Jets were constructed at this stage using anti-kT algorithm [89]. The ATLAS Collaboration has recently included the same-sign trilepton channel in their search for stop quarks in the context of MSSM [28]. We have implemented the same analysis to obtain our signal rate. The stop production cross-section has been appropriately scaled using the next-to-leading-order (NLO) factor obtained from the LHC SUSY cross-section working group webpage [90].

The electrons are primarily selected with  $p_T > 10$  GeV and  $|\eta| < 2.47$  barring the region between the barrel and endcap electromagnetic calorimeters,  $1.37 < |\eta| < 1.52$ . The muon candidates are selected with the same  $p_T$  threshold and  $|\eta| < 2.5$ . Jets are reconstructed with radius  $R = 0.4$ ,  $p_T > 20$  GeV and  $|\eta| < 2.8$ . In our analysis we have implemented the  $p_T$  dependent b-jet tagging efficiency and light jet misidentification efficiency following the ATLAS Collaboration criteria [28]. Finally, the b-jets are counted with  $|\eta| < 2.5$ . The event selection further requires at least two of the three same-sign leptons have  $p_T > 20$  GeV. In order to reduce SM backgrounds arising from mismeasurement of electron charge, events are vetoed if invariant mass of two same-sign electrons is within a 10 GeV window of the  $Z$ -boson mass. The ATLAS Collaboration has obtained  $1.6 \pm 0.8$  SM background events at 13 TeV LHC with these criteria in the  $\ell^\pm \ell^\pm \ell^\pm + \geq 1$  b-jet signal region with an integrated luminosity of  $36 \text{ fb}^{-1}$  [28]. In Table II below, we have shown the signal cross-section corresponding to our benchmark points and also the required luminosity to probe this scenario with  $3\sigma$  and  $5\sigma$  statistical significance ( $\mathcal{S}$ ). In order to compute  $\mathcal{S}$  of our signal ( $S$ ) over the SM background ( $B$ ) we have used  $\mathcal{S} = \frac{S}{\sqrt{B + \sigma_B^2}}$ , where  $\sigma_B$  is the uncertainty in the measurement of the SM background. For simplicity, even for the higher luminosity estimates, we have assumed that  $\sigma_B$  remains the same fraction of  $B$  as it is in  $36 \text{ fb}^{-1}$  integrated luminosity<sup>7</sup>. Note that, the IH scenario for BP1 can already be ruled out from the accumulated data. However, the NH case needs an integrated luminosity  $\sim 828.3 \text{ fb}^{-1}$  to achieve a  $3\sigma$  statistical significance. BP2, on the other hand, would require much higher luminosity owing to the larger stop mass. A discovery significance in the NH case is beyond the reach of even  $3000 \text{ fb}^{-1}$  integrated luminosity. However, for the IH case,  $\mathcal{S} = 3\sigma$  can be achieved at  $\sim 845.8 \text{ fb}^{-1}$ .

Results	BP1		BP2	
	Normal	Inverted	Normal	Inverted
$\sigma_{\text{sig}}$ (fb)	0.070	0.193	0.026	0.070
Required $\mathcal{L}$ ( $\text{fb}^{-1}$ ) ( $3\sigma$ )	828.3	12.2	> 3000	845.8
Required $\mathcal{L}$ ( $\text{fb}^{-1}$ ) ( $5\sigma$ )	> 3000	44.6	> 3000	> 3000

TABLE II. Signal cross-section and required integrated luminosity at 13 TeV LHC to probe the benchmark points with  $3\sigma$  and  $5\sigma$  statistical significance in the  $\ell^\pm \ell^\pm \ell^\pm + \geq 1$  b-jet signal region.

As evident from Table II, the stop mass probe in the present scenario depends heavily on the choice of neutrino mass hierarchy due to the variation in  $\text{BR}(\tilde{\chi}_1^\pm \rightarrow \ell \tilde{\nu}_{1,2})$ . For more comprehensive understanding of the parameter space, we have used the existing LHC data in order to determine the exclusion limit on the lighter stop mass subjected to NH and IH in the light neutrino masses. For this, we have kept the relative separation of the masses uniform throughout, i.e.,  $m_{\tilde{\chi}_2^0} \leq m_{\tilde{t}_1} - m_t$  and  $m_h \geq m_{\tilde{\chi}_2^0} - m_{\tilde{\chi}_1^\pm} (m_{\tilde{\chi}_1^0}) \geq m_W$ . The simple requirement of our signal region makes sure that the cuts efficiency does not vary significantly with such choice of the spectrum over a wide range of stop mass.

In Fig. 3 we have shown the choice of our mass spectra in the framework of SISM under consideration and presented reach of stop masses with existing data at the 13 TeV LHC with  $36 \text{ fb}^{-1}$  luminosity data. The red horizontal line represents the 95% confidence level exclusion limit on the visible cross-section ( $\sigma_{\text{vis.}} = 0.11 \text{ fb}$ ) in this signal region put by the ATLAS collaboration [28]. The violet and cyan lines represent the stop mass reach in our model framework subjected to the existing data with IH and NH choices in the light neutrino masses respectively with the shaded regions already excluded. As evident,  $m_{\tilde{t}_1} < 815$  and  $935$  GeV are already excluded under the NH and IH assumptions respectively.

If some excess is found in this signal region at higher luminosity, it would be useful to have a prior idea of the mass range in which we can hope to discover the stop with certainty. In order to determine this, we have computed the

<sup>7</sup> This is a forced choice we had to make due to lack of information resulting in a conservative estimate.

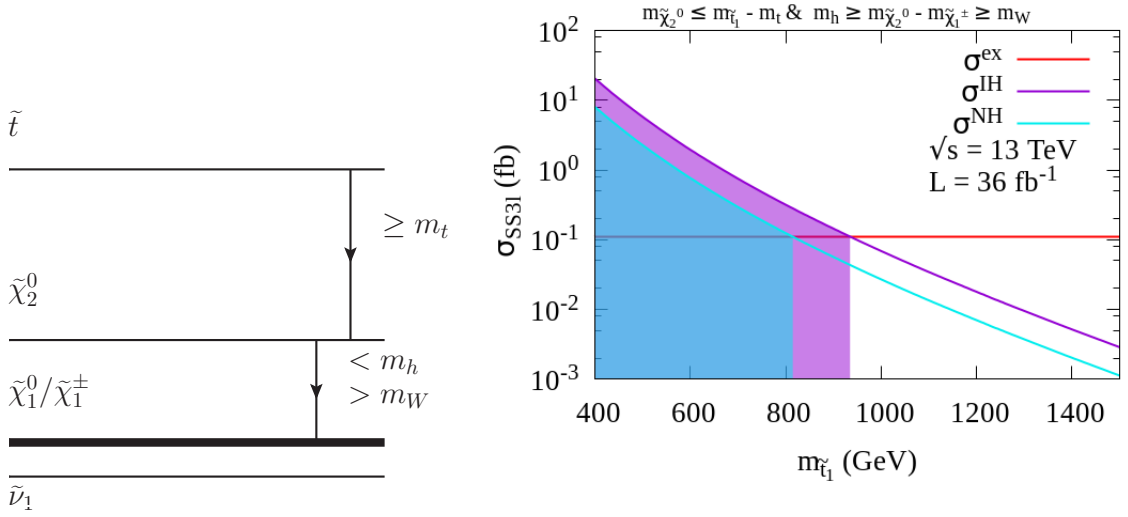


FIG. 3. On the left: Choice of mass spectra. On the right: The expected cross-section in the same-sign tri-lepton final state vs the stop mass and the exclusion obtained from the  $36 \text{ fb}^{-1}$  luminosity data at the LHC. The red horizontal line corresponds to the experimental limit on the visible cross-section [28].

discovery significance of the stop quark lying within the mass range [700 GeV - 1.2 TeV] at two different luminosities,  $130 \text{ fb}^{-1}$  and  $3000 \text{ fb}^{-1}$  with  $\sqrt{s} = 13 \text{ TeV}$ . Fig. 4 shows the distribution of the obtained statistical significance as a function of  $m_{\tilde{t}_1}$ . The horizontal grey lines in the figure represent the coveted  $3\sigma$  and  $5\sigma$  statistical significance requirements. The violet and cyan solid lines represent the prospects of our scenario subjected to the IH and NH choices. The dotted lines around the solid ones are obtained assuming a 10% variation in  $\sigma_B$ . As evident from Fig. 4, at low luminosity ( $130 \text{ fb}^{-1}$ ), the discovery reach of  $m_{\tilde{t}_1}$  can be upto  $\sim 970 \text{ GeV}$  at most whereas, the high luminosity ( $3000 \text{ fb}^{-1}$ ) option can slightly improve the mass range upto  $\sim 1 \text{ TeV}$ . If IH in the neutrino masses is ruled out in future by the neutrino oscillation experiments,  $m_{\tilde{t}_1}$  discovery reach can not be beyond 900 GeV even at large luminosity at the LHC.

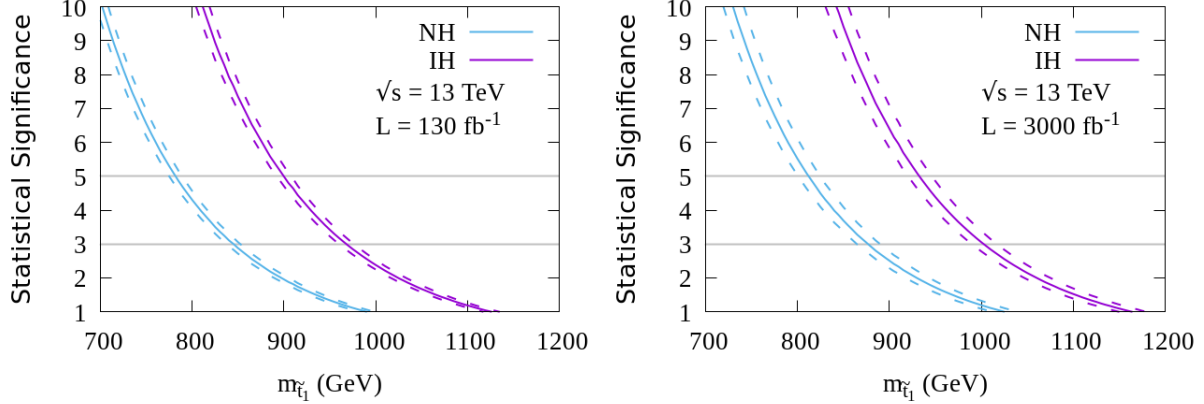


FIG. 4. Discovery reach in the stop mass plane at  $\sqrt{s} = 13 \text{ TeV}$  LHC with two choices of integrated luminosity,  $130 \text{ fb}^{-1}$  and  $3000 \text{ fb}^{-1}$ . The parallel grey lines indicate  $3\sigma$  and  $5\sigma$  statistical significance.

In spite of the small signal cross-section, therefore, the stop mass discovery reach can be in the TeV range in this signal region owing to the small SM background. The results do not improve drastically with the increase in the luminosity because of the presence of a large uncertainty factor in the SM background estimation. With more accumulation of data the statistical error is expected to decrease and that can improve the stop discovery reach significantly. With a high center-of-mass energy hadron collider becoming more and more relevant in the context of SUSY search, we have also estimated a projected discovery reach of the stop mass in the present scenario at a 27 TeV pp collider. Our SM background computation at this centre-of-mass energy from  $t\bar{t}h$ ,  $t\bar{t}W$ ,  $t\bar{t}Z(\gamma)$ ,  $VV$  and  $VVV$ ,

where  $V$  represents gauge bosons ( $W$  and  $Z$ ) production channels yields a cross-section of 0.077 fb. We have computed  $\sigma_B$  following the same prescription as in Fig. 4. The NLO k-factor has been computed with Prospino [91, 92] The  $\sqrt{s} = 27$  TeV results are shown in Fig. 5. The increase in the signal cross-section improves the discovery reach of  $m_{\tilde{\tau}_1} \sim 1.55$  TeV and  $\sim 1.45$  TeV for IH and NH choices respectively.

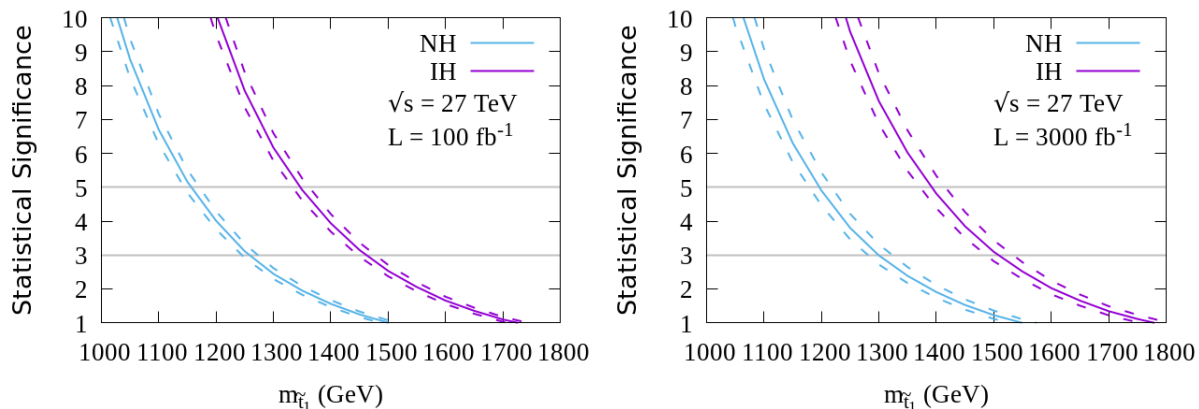


FIG. 5. Discovery reach in the stop mass plane at  $\sqrt{s} = 27$  TeV LHC with two choices of integrated luminosity,  $100 \text{ fb}^{-1}$  and  $3000 \text{ fb}^{-1}$ . Color codings are similar to Fig. 4.

## V. SUMMARY AND CONCLUSION

In this work, we have investigated the interplay among neutrino mass mechanism, DM requirements and stop search at the LHC in the context of supersymmetric inverse seesaw scenario. The SISM scenario naturally gives rise to a right-sneutrino DM in the theory in the form of the LSP within an R-parity conserving framework. Originating from a gauge singlet, the sneutrino requires to lie close to the 125 GeV Higgs resonance annihilation in order to produce correct relic density. However, the present DM direct detection constraints have put this parameter space in jeopardy forcing us to look for co-annihilation of the right-sneutrino DM.

The sneutrino interactions are driven by the same Dirac neutrino Yukawa couplings introduced to fit the neutrino oscillation data. We have shown, using Casas-Ibarra parameterization, that the lepton flavor violating constraints force these Yukawa parameters to be small. The choice of  $yY_\nu$  here is subjected to the choice of heavy neutrino mass and the lepton number violating parameter,  $\mu_S$ . Thus the LFV constraints put a limit on the choices of  $\mu_S \gtrsim 10^{-6}$  GeV for sub-TeV heavy neutrino masses in particular for IH. Among the constraints arising from the decay,  $\mu \rightarrow e\gamma$  turns out to be the most severe. The predictions for  $\tau \rightarrow \mu\gamma$ , and  $\tau \rightarrow \mu\mu\mu$  are relatively weaker, and constrain sneutrino mass only in the  $m_{\tilde{\nu}} \lesssim 100$  GeV range. The model predictions in the  $\tau$  sector can be tested in the future LFV searches. The constrained  $Y_\nu$  from the LFV data results in a very small direct detection cross-section of the sneutrino, which is beyond the present DM experimental sensitivity by a few orders of magnitude. This also forces the resonant contribution in relic density to be small and motivates one to look for co-annihilation of the sneutrino DM with other particles. In this work, we have explored the sneutrino-wino co-annihilation which has interesting implications for stop search at the LHC.

The co-annihilating DM scenario gives rise to a partially compressed electroweak spectra which makes the conventional stop search strategies weaker. We have shown that the relic density is satisfied due to co-annihilation of sneutrino with wino like neutralino, and chargino, requiring the mass difference between the LSP and chargino/neutralino to be  $\Delta m \sim 15 - 30$  GeV for all values of sneutrino masses in between 100-1000 GeV. Indirect limit on the LSP sneutrino mass arises from the wino mass bounds. However, the compression in the spectra again results in relatively weaker exclusions allowing the LSP to be as light as 200 GeV in this scenario.

Under such circumstances, conventional stop search strategies prove to be ineffective in probing TeV scale stop masses. Here we have studied stop pair production and its subsequent decays into top and a bino-like NNLSP  $\tilde{\chi}_2^0$ . Further decay of the bino into gauge boson and a wino-like chargino  $\tilde{\chi}^\pm$ , and  $\tilde{\chi}^\pm \rightarrow \ell\tilde{\nu}_{1,2}$  leads to a novel same-sign triplepton signal  $\ell^\pm\ell^\pm\ell^\pm + \geq 1b - \text{jets} + \cancel{E_T}$  for the stop at LHC. Unlike the conventional stop search channels, this signal region has very small SM background. As a result, despite of the small signal rate, stop mass can be probed close to 935 (815) GeV with the existing LHC data for IH (NH) choices in neutrino mass hierarchy. Stop mass limits

prove to be stronger for the inverted hierarchy in the light neutrino masses due to the greater leptonic branching ratio of the chargino resulting in greater abundance of electrons in the final state, which also serves as a distinguishing feature of this model from the MSSM. In the MSSM with neutralino LSP, however, this same-sign trilepton signal rate will be much lower. A  $3\sigma$  discovery significance can be obtained with  $m_{\tilde{\tau}_1} \sim 1$  TeV at high luminosity with 13 TeV center-of-mass energy. We have also shown that the stop mass discovery reach can go beyond 1.5 TeV at a high-energy pp collider with 27 TeV center-of-mass energy. With improved sensitivity in SM background measurement at higher luminosity, the conservative limits we obtained are bound to improve significantly.

## VI. ACKNOWLEDGEMENT

SM and KH acknowledge H2020-MSCA-RICE-2014 grant no. 645722 (NonMinimal Higgs). SM would like to thank IACS, Kolkata for hospitality during the final phase of this work. M.M. would like to acknowledge the DST-INSPIRE research grant IFA14-PH-99.

- 
- [1] M. C. Gonzalez-Garcia, M. Maltoni, and T. Schwetz, Nucl. Phys. **B908**, 199 (2016), arXiv:1512.06856 [hep-ph].
- [2] P. F. de Salas, D. V. Forero, C. A. Ternes, M. Tortola, and J. W. F. Valle, (2017), arXiv:1708.01186 [hep-ph].
- [3] P. Minkowski, Phys. Lett. **B67**, 421 (1977).
- [4] T. Yanagida, In Proceedings of the Workshop on the Baryon Number of the Universe and Unified Theories, Tsukuba, Japan, 13-14 Feb 1979.
- [5] R. N. Mohapatra and G. Senjanovic, Phys. Rev. Lett. **44**, 912 (1980).
- [6] S. L. Glashow, NATO Adv. Study Inst. Ser. B Phys. **59**, 687 (1980).
- [7] M. Gell-Mann, P. Ramond, and R. Slansky, Print-80-0576 (CERN).
- [8] R. N. Mohapatra, Phys. Rev. Lett. **56**, 561 (1986).
- [9] R. N. Mohapatra and J. W. F. Valle, *Sixty years of double beta decay: From nuclear physics to beyond standard model particle physics*, Phys. Rev. **D34**, 1642 (1986), [,235(1986)].
- [10] M. C. Gonzalez-Garcia and J. W. F. Valle, Phys. Lett. **B216**, 360 (1989).
- [11] A. Das and N. Okada, Phys. Rev. **D88**, 113001 (2013), arXiv:1207.3734 [hep-ph].
- [12] A. Das and N. Okada, Phys. Rev. **D93**, 033003 (2016), arXiv:1510.04790 [hep-ph].
- [13] A. Das and N. Okada, Phys. Lett. **B774**, 32 (2017), arXiv:1702.04668 [hep-ph].
- [14] H.-S. Lee, K. T. Matchev, and S. Nasri, Phys. Rev. **D76**, 041302 (2007), arXiv:hep-ph/0702223 [HEP-PH].
- [15] D. G. Cerdeno, C. Munoz, and O. Seto, Phys. Rev. **D79**, 023510 (2009), arXiv:0807.3029 [hep-ph].
- [16] S. Mondal, S. Biswas, P. Ghosh, and S. Roy, JHEP **05**, 134 (2012), arXiv:1201.1556 [hep-ph].
- [17] P. S. Bhupal Dev, S. Mondal, B. Mukhopadhyaya, and S. Roy, JHEP **09**, 110 (2012), arXiv:1207.6542 [hep-ph].
- [18] V. De Romeri and M. Hirsch, JHEP **12**, 106 (2012), arXiv:1209.3891 [hep-ph].
- [19] S. Banerjee, P. S. B. Dev, S. Mondal, B. Mukhopadhyaya, and S. Roy, JHEP **10**, 221 (2013), arXiv:1306.2143 [hep-ph].
- [20] D. K. Ghosh, S. Mondal, and I. Saha, JCAP **1502**, 035 (2015), arXiv:1405.0206 [hep-ph].
- [21] J. Chang, K. Cheung, H. Ishida, C.-T. Lu, M. Spinrath, and Y.-L. S. Tsai, JHEP **10**, 039 (2017), arXiv:1707.04374 [hep-ph].
- [22] J. Chang, K. Cheung, H. Ishida, C.-T. Lu, M. Spinrath, and Y.-L. S. Tsai, (2018), arXiv:1806.04468 [hep-ph].
- [23] L. Delle Rose, S. Khalil, S. J. D. King, C. Marzo, S. Moretti, and C. S. Un, Phys. Rev. **D96**, 055004 (2017), arXiv:1702.01808 [hep-ph].
- [24] L. Delle Rose, S. Khalil, S. J. D. King, S. Kulkarni, C. Marzo, S. Moretti, and C. S. Un, JHEP **07**, 100 (2018), arXiv:1712.05232 [hep-ph].
- [25] L. Delle Rose, S. Khalil, S. J. D. King, S. Kulkarni, C. Marzo, S. Moretti, and C. S. Un (2018) arXiv:1804.09470 [hep-ph].
- [26] T. Falk, K. A. Olive, and M. Srednicki, Phys. Lett. **B339**, 248 (1994), arXiv:hep-ph/9409270 [hep-ph].
- [27] T. Hebbeker, Phys. Lett. **B470**, 259 (1999), arXiv:hep-ph/9910326 [hep-ph].
- [28] M. Aaboud *et al.* (ATLAS), JHEP **09**, 084 (2017), arXiv:1706.03731 [hep-ex].
- [29] M. Aaboud *et al.* (ATLAS), JHEP **08**, 006 (2017), arXiv:1706.03986 [hep-ex].
- [30] M. Aaboud *et al.* (ATLAS), Eur. Phys. J. **C77**, 898 (2017), arXiv:1708.03247 [hep-ex].
- [31] M. Aaboud *et al.* (ATLAS), JHEP **11**, 195 (2017), arXiv:1708.09266 [hep-ex].
- [32] M. Aaboud *et al.* (ATLAS), JHEP **12**, 085 (2017), arXiv:1709.04183 [hep-ex].
- [33] M. Aaboud *et al.* (ATLAS), (2017), arXiv:1711.11520 [hep-ex].
- [34] M. Aaboud *et al.* (ATLAS), (2018), arXiv:1803.10178 [hep-ex].
- [35] F. F. Deppisch, P. S. Bhupal Dev, and A. Pilaftsis, New J. Phys. **17**, 075019 (2015), arXiv:1502.06541 [hep-ph].
- [36] S. Khalil, Phys. Rev. **D82**, 077702 (2010), arXiv:1004.0013 [hep-ph].
- [37] P. S. B. Dev and R. N. Mohapatra, Phys. Rev. **D81**, 013001 (2010), arXiv:0910.3924 [hep-ph].
- [38] F. Deppisch and J. W. F. Valle, Phys. Rev. **D72**, 036001 (2005), arXiv:hep-ph/0406040 [hep-ph].
- [39] M. Hirsch, T. Kernreiter, J. C. Romao, and A. Villanova del Moral, JHEP **01**, 103 (2010), arXiv:0910.2435 [hep-ph].

- [40] A. Abada, D. Das, A. Vicente, and C. Weiland, *JHEP* **09**, 015 (2012), arXiv:1206.6497 [hep-ph].
- [41] A. Abada, M. E. Krauss, W. Porod, F. Staub, A. Vicente, and C. Weiland, *JHEP* **11**, 048 (2014), arXiv:1408.0138 [hep-ph].
- [42] J. A. Casas and A. Ibarra, *Nucl. Phys.* **B618**, 171 (2001), arXiv:hep-ph/0103065 [hep-ph].
- [43] K.-S. Sun, T.-F. Feng, G.-H. Luo, X.-Y. Yang, and J.-B. Chen, *Mod. Phys. Lett.* **A28**, 1350151 (2013), arXiv:1312.2073 [hep-ph].
- [44] X. Marciano, *Lepton flavor violation from low scale seesaw neutrinos with masses reachable at the LHC*, Ph.D. thesis, Madrid, Autonoma U. (2017), arXiv:1710.08032 [hep-ph].
- [45] L. Lello and D. Boyanovsky, *Phys. Rev.* **D87**, 073017 (2013), arXiv:1208.5559 [hep-ph].
- [46] A. Blondel, E. Graverini, N. Serra, and M. Shaposhnikov (FCC-ee study Team), *Proceedings, 37th International Conference on High Energy Physics (ICHEP 2014): Valencia, Spain, July 2-9, 2014*, *Nucl. Part. Phys. Proc.* **273-275**, 1883 (2016), arXiv:1411.5230 [hep-ex].
- [47] M. Anelli *et al.* (SHiP), (2015), arXiv:1504.04956 [physics.ins-det].
- [48] A. Abada, D. Das, and C. Weiland, *JHEP* **03**, 100 (2012), arXiv:1111.5836 [hep-ph].
- [49] J. Adam *et al.* (MEG), *Phys. Rev. Lett.* **110**, 201801 (2013), arXiv:1303.0754 [hep-ex].
- [50] A. M. Baldini *et al.*, (2013), arXiv:1301.7225 [physics.ins-det].
- [51] B. Aubert *et al.* (BaBar), *Phys. Rev. Lett.* **104**, 021802 (2010), arXiv:0908.2381 [hep-ex].
- [52] T. Aushev *et al.*, (2010), arXiv:1002.5012 [hep-ex].
- [53] K. Hayasaka *et al.*, *Phys. Lett.* **B687**, 139 (2010), arXiv:1001.3221 [hep-ex].
- [54] W. H. Bertl *et al.* (SINDRUM II), *Eur. Phys. J.* **C47**, 337 (2006).
- [55] L. Bartoszek *et al.* (Mu2e), (2014), arXiv:1501.05241 [physics.ins-det].
- [56] W. Porod, *Comput. Phys. Commun.* **153**, 275 (2003), arXiv:hep-ph/0301101 [hep-ph].
- [57] W. Porod and F. Staub, *Comput. Phys. Commun.* **183**, 2458 (2012), arXiv:1104.1573 [hep-ph].
- [58] W. Porod, *JHEP* **05**, 030 (2002), arXiv:hep-ph/0202259 [hep-ph].
- [59] F. Staub, (2008), arXiv:0806.0538 [hep-ph].
- [60] F. Staub, *Comput. Phys. Commun.* **181**, 1077 (2010), arXiv:0909.2863 [hep-ph].
- [61] F. Staub, *Comput. Phys. Commun.* **182**, 808 (2011), arXiv:1002.0840 [hep-ph].
- [62] F. Staub, *Comput. Phys. Commun.* **185**, 1773 (2014), arXiv:1309.7223 [hep-ph].
- [63] F. Staub, *Adv. High Energy Phys.* **2015**, 840780 (2015), arXiv:1503.04200 [hep-ph].
- [64] P. Adamson *et al.* (NOvA), *Phys. Rev. Lett.* **118**, 231801 (2017), arXiv:1703.03328 [hep-ex].
- [65] M. A. Acero *et al.* (NOvA), (2018), arXiv:1806.00096 [hep-ex].
- [66] G. Hinshaw *et al.* (WMAP), *Astrophys. J. Suppl.* **208**, 19 (2013), arXiv:1212.5226 [astro-ph.CO].
- [67] E. Aprile *et al.* (XENON), *Phys. Rev. Lett.* **119**, 181301 (2017), arXiv:1705.06655 [astro-ph.CO].
- [68] X. Cui *et al.* (PandaX-II), *Phys. Rev. Lett.* **119**, 181302 (2017), arXiv:1708.06917 [astro-ph.CO].
- [69] E. Aprile *et al.* (XENON), (2018), arXiv:1805.12562 [astro-ph.CO].
- [70] C. Arina and M. E. Cabrera, *JHEP* **04**, 100 (2014), arXiv:1311.6549 [hep-ph].
- [71] G. Belanger, F. Boudjema, A. Pukhov, and A. Semenov, *Comput. Phys. Commun.* **185**, 960 (2014), arXiv:1305.0237 [hep-ph].
- [72] M. Aaboud *et al.* (ATLAS), (2018), arXiv:1803.02762 [hep-ex].
- [73] A. M. Sirunyan *et al.* (CMS), (2018), arXiv:1801.03957 [hep-ex].
- [74] M. Aaboud *et al.* (ATLAS), *Phys. Rev.* **D97**, 052010 (2018), arXiv:1712.08119 [hep-ex].
- [75] M. Aaboud *et al.* (ATLAS), (2017), arXiv:1712.02118 [hep-ex].
- [76] A. M. Sirunyan *et al.* (CMS), (2017), arXiv:1709.05406 [hep-ex].
- [77] M. Aaboud *et al.* (ATLAS), *Eur. Phys. J.* **C78**, 154 (2018), arXiv:1708.07875 [hep-ex].
- [78] A. M. Sirunyan *et al.* (CMS), *JHEP* **11**, 029 (2017), arXiv:1706.09933 [hep-ex].
- [79] M. Drees, H. Dreiner, D. Schmeier, J. Tattersall, and J. S. Kim, *Comput. Phys. Commun.* **187**, 227 (2015), arXiv:1312.2591 [hep-ph].
- [80] D. Dercks, N. Desai, J. S. Kim, K. Rolbiecki, J. Tattersall, and T. Weber, *Comput. Phys. Commun.* **221**, 383 (2017), arXiv:1611.09856 [hep-ph].
- [81] J. Alwall, M. Herquet, F. Maltoni, O. Mattelaer, and T. Stelzer, *JHEP* **06**, 128 (2011), arXiv:1106.0522 [hep-ph].
- [82] J. Alwall, R. Frederix, S. Frixione, V. Hirschi, F. Maltoni, O. Mattelaer, H. S. Shao, T. Stelzer, P. Torrielli, and M. Zaro, *JHEP* **07**, 079 (2014), arXiv:1405.0301 [hep-ph].
- [83] T. Sjöstrand, S. Ask, J. R. Christiansen, R. Corke, N. Desai, P. Ilten, S. Mrenna, S. Prestel, C. O. Rasmussen, and P. Z. Skands, *Comput. Phys. Commun.* **191**, 159 (2015), arXiv:1410.3012 [hep-ph].
- [84] R. D. Ball *et al.*, *Nucl. Phys.* **B867**, 244 (2013), arXiv:1207.1303 [hep-ph].
- [85] R. D. Ball *et al.* (NNPDF), *JHEP* **04**, 040 (2015), arXiv:1410.8849 [hep-ph].
- [86] J. de Favereau, C. Delaere, P. Demin, A. Giammanco, V. Lemaître, A. Mertens, and M. Selvaggi (DELPHES 3), *JHEP* **02**, 057 (2014), arXiv:1307.6346 [hep-ex].
- [87] M. Selvaggi, *Proceedings, 15th International Workshop on Advanced Computing and Analysis Techniques in Physics Research (ACAT 2013)*, *J. Phys. Conf. Ser.* **523**, 012033 (2014).
- [88] A. Mertens, *Proceedings, 16th International workshop on Advanced Computing and Analysis Techniques in physics (ACAT 14)*, *J. Phys. Conf. Ser.* **608**, 012045 (2015).
- [89] M. Cacciari, G. P. Salam, and G. Soyez, *JHEP* **04**, 063 (2008), arXiv:0802.1189 [hep-ph].
- [90] <https://twiki.cern.ch/twiki/bin/view/LHCPhysics/SUSYCrossSections>.
- [91] W. Beenakker, R. Hopker, and M. Spira, (1996), arXiv:hep-ph/9611232 [hep-ph].

[92] W. Beenakker, M. Kramer, T. Plehn, M. Spira, and P. M. Zerwas, Nucl. Phys. **B515**, 3 (1998), arXiv:hep-ph/9710451 [hep-ph].